
DP-IQA: Utilizing Diffusion Prior for Blind Image Quality Assessment in the Wild

Honghao Fu^{1*} Yufei Wang^{1*} Wenhan Yang² Bihan Wen^{1†}

¹ Nanyang Technological University, Singapore

¹ PengCheng Laboratory, China

{hfu006, yufei001, bihan.wen}@ntu.edu.sg yangwh@pcl.ac.cn

<https://github.com/RomGai/DP-IQA>

Abstract

Image quality assessment (IQA) plays a critical role in selecting high-quality images and guiding compression and enhancement methods in a series of applications. The blind IQA, which assesses the quality of in-the-wild images containing complex authentic distortions without reference images, poses greater challenges. Existing methods are limited to modeling a uniform distribution with local patches and are bothered by the gap between low and high-level visions (caused by widely adopted pre-trained classification networks). In this paper, we propose a novel IQA method called diffusion priors-based IQA (DP-IQA), which leverages the prior knowledge from the pre-trained diffusion model with its excellent powers to bridge semantic gaps in the perception of the visual quality of images. Specifically, we use pre-trained stable diffusion as the backbone, extract multi-level features from the denoising U-Net during the upsampling process at a specified timestep, and decode them to estimate the image quality score. The text and image adapters are adopted to mitigate the domain gap for downstream tasks and correct the information loss caused by the variational autoencoder bottleneck. Finally, we distill the knowledge in the above model into a CNN-based student model, significantly reducing the parameter to enhance applicability, with the student model performing similarly or even better than the teacher model surprisingly. Experimental results demonstrate that our DP-IQA achieves state-of-the-art results on various in-the-wild datasets with better generalization capability, which shows the superiority of our method in global modeling and utilizing the hierarchical feature clues of diffusion for evaluating image quality.

1 Introduction

Millions of images are uploaded to social media platforms and spread across the internet daily [31]. Inevitably, some images are of poor quality, posing annoyances due to the negative impression they convey to the viewing audience [5]. Image Quality Assessment (IQA) [45] aims to assess the visual quality of images from the human visual perspectives. It is essential to guide the optimization or operation of compression and enhancement techniques, for guaranteeing high-quality image content for a series of applications, *e.g.* social media sharing, and media streaming, *etc.* Therefore, robustness and generalization of IQA methods against various real-world distortions significantly have a huge impact on the display of billions of images to the public.

IQA methods are typically categorized based on reference image availability into: (1) full-reference (FR), which uses an undistorted high-quality reference image, and (2) no-reference (NR), which

* means equal contribution, and † means corresponding author.

does not rely on any reference. Currently, IQA techniques are primarily applied to images collected in real-world environments, known as “in-the-wild images”. In-the-wild IQA is more challenging than the one handling distorted images with given kinds of distortion due to various unpredictable distortions, also termed authentic distortions. FR methods are limited in in-the-wild scenarios where undistorted references are hard to come by. Hence, NR methods, also referred to as blind IQA (BIQA), have emerged as a promising research direction, capable of directly predicting image quality without references. However, due to the lack of reference information and the diversity of image content, the NR condition also presents significant challenges.

There is another challenge for NR IQA, *i.e.* how to better learn image quality features from limited data. It is quite laborious to create NR IQA datasets requiring multiple volunteers to provide subjective scores for the same set of distorted images, which cost much effort compared with image datasets for analytics vision tasks [20]. Recent BIQA methods often split images into patches with identical quality scores for data augmentation [3, 16, 24, 25, 38, 45, 48], which neglects global semantics and has to assume uniform distortion distribution across an image. This assumption leads to the methodology of synthesizing distorted images in the training, resulting in distortions and assessments that do not well align with human perception of in-the-wild images. Besides, some methods [2, 10, 23, 38, 45, 53] leverage priors from pre-trained image classification models, which focus on high-level vision and lack sufficient low-level information. Therefore, existing BIQA methods still show limitations in dealing with authentic distortions in in-the-wild images.

To address these issues, we propose using a pre-trained diffusion model as the backbone for IQA. Diffusion models excel in image understanding and global modeling due to their probabilistic density modeling and progressive approximation learning strategies. In this paper, we have fully tapped into the potential of diffusion models and adapted them better suited for in-the-wild image quality assessment with non-uniform distortion and quality distribution without using patch-wise assemble architecture. Compared to classification models pre-trained on smaller datasets like ImageNet [6] (*e.g.*, ResNet-50 [18]), diffusion models trained on more extensive datasets like LAION-5B [46] offer richer prior knowledge (*e.g.*, stable diffusion, SD [41]). The priors from large-scale pre-trained diffusion models have found widespread use in high-level tasks like image classification [27] and semantic segmentation [52, 63], as well as low-level tasks like super-resolution [54] and image restoration [9, 17, 55]. However, despite their advantages, diffusion models typically require multiple denoising iterations for modeling. Unlike adapting the output layer of a classification model for IQA score regression directly, it is still unclear to extract what features from diffusion models and how to utilize them effectively.

In this paper, we propose a novel BIQA method called diffusion prior-based IQA (DP-IQA). It leverages pre-trained stable diffusion as the backbone, extracting multi-level features from the denoising U-Net during the upsampling process at a specific timestep and decoding them to estimate image quality. The text and image adapters are adopted to mitigate the domain gap in the text encoder for downstream tasks and correct the information loss caused by the variational autoencoder bottleneck [11, 63, 64]. DP-IQA processes the entire in-the-wild image, avoiding patch splitting and thus capturing global information about distortion and quality distribution. Moreover, we distill the knowledge in the above model into a CNN-based student model, significantly reducing the parameter to enhance applicability. Experiments demonstrate DP-IQA’s state-of-the-art (SOTA) performance and superior generalization on various in-the-wild datasets. To the best of our knowledge, DP-IQA is the first method to apply diffusion priors in IQA tasks.

2 Related Works

2.1 Blind image quality assessment

Traditional BIQA primarily leverages statistical features from the spatial and transform domains of images using natural scene statistics [12, 15, 33, 34] and employs machine learning models for the regression of image quality score [42, 44, 56]. However, these methods often fail to capture high-level image information due to their reliance on specific feature computations. Recently, deep learning has advanced BIQA significantly [13, 21, 51, 57, 60, 62, 65]. Initial methods used Convolutional Neural Networks (CNNs) to learn image quality features [24, 30, 36], but the limited scale of IQA datasets hindered the models’ representational capabilities. Improvements included augmenting data by splitting images into multiple patches [3, 24, 25, 48] and fine-tuning classification models

pre-trained on larger-scale image datasets like ImageNet [2, 10, 53]. However, as discussed in Sec.1, these strategies yield suboptimal results. Early generative models, including Generative Adversarial Networks (GANs)[29, 40, 66], have been used for BIQA tasks. The methods based on GANs typically reconstruct an undistorted image from a distorted one, then extract features from this process, or use the reconstructed image as a reference for IQA. Consequently, they still require undistorted reference images during training, limiting their applicability to in-the-wild images without reference.

With the introduction of the more powerful Vision Transformer (ViT) [7], recent BIQA works [16, 23, 38, 58, 61] mostly leverage ViT for better performance. For instance, MUSIQ[23] fine-tunes a ViT pre-trained on classification task on ImageNet[6] to learn image patches’ quality features and spatial relationships, while LIQE[61] refines the ViT-based CLIP model to classify image quality levels based on the CLIP [39] similarity between text prompts and image patches. However, recent SOTA methods[16, 23, 38, 45, 61] still require patch splitting or fine-tuning of pre-trained classification networks. Addressing these issues, we globally models in-the-wild images and incorporates low-level prior knowledge that has been overlooked in previous work.

2.2 Diffusion model priors

Diffusion-based generative models excel in generating high-quality images with intricate scenes and semantics from textual descriptions, demonstrating a profound understanding of text and vision. The prior knowledge embedded in large-scale pre-trained diffusion models like Stable Diffusion [41] has proven effective for high-level visual tasks such as image classification [27], semantic segmentation [52, 63], and depth estimation [22, 63]. Additionally, it has also been utilized in low-level tasks like super-resolution [54] and image restoration [9, 17, 55], showing impressive results. This indicates that pre-trained diffusion models encompass rich high-level and low-level priors, which we utilize to supplement the low-level priors lacking in past BIQA works that rely on pre-trained classification models. However, diffusion models have a large number of parameters and incur high computational cost, hindering their deployment and application in real-world scenarios. Thus, we also distill the knowledge from the trained DP-IQA model into a smaller pre-trained vision model.

3 Method

3.1 Preliminary

Diffusion. As the backbone of our proposed DP-IQA, we first provide a brief introduction to the principles of diffusion models. Let z_t be the random noise at the t -th timestep. Diffusion models transform z_t to the denoised sample z_0 by gradually denoising z_t to a less noisy z_{t-1} . The forward diffusion process is modeled as:

$$q(z_t | z_{t-1}) = \mathcal{N}(z_t; \sqrt{\alpha_t} z_{t-1}, (1 - \alpha_t)\mathbf{I}), \quad (1)$$

where $\{\alpha_t\}$ are fixed coefficients that determine the noise schedule. Define $\bar{\alpha}_t = \prod_{s=1}^t \alpha_s$. z_t can also be obtained directly from z_0 [1]:

$$q(z_t | z_0) = \mathcal{N}(z_t; \sqrt{\bar{\alpha}_t} z_0, (1 - \bar{\alpha}_t)\mathbf{I}), \quad (2)$$

$$z_t = \sqrt{\bar{\alpha}_t} z_0 + \sqrt{1 - \bar{\alpha}_t} \epsilon, \quad \epsilon \sim \mathcal{N}(0, \mathbf{I}). \quad (3)$$

This makes sampling for any z_t more efficient. With proper re-parameterization, the training objective of diffusion models can be derived as [19, 63]:

$$\mathcal{L}_{\text{DM}} = \mathbb{E}_{z_0, \epsilon, t} [\|\epsilon - \epsilon_\theta(z_t(z_0, \epsilon), t; \mathcal{C})\|_2^2], \quad (4)$$

where ϵ_θ is a denoising autoencoder that is learned to predict ϵ given the conditional embedding \mathcal{C} . In our task, the denoising autoencoder ϵ_θ is a U-Net, z_t is a latent representation of a distorted image, which can also be regarded as a latent variable that has not been fully denoised from random noise. By controlling the conditional embedding \mathcal{C} , we enable the denoising U-Net to effectively focus on the target features in z_t , and thereby extract the prior knowledge required for the IQA task from a single timestep in the diffusion process.

3.2 Overview

In this paper, we aim to address the challenges of **adapting diffusion model backbones and priors for IQA of in-the-wild images**, to bridge the gap between limited kinds of **synthetic visual**

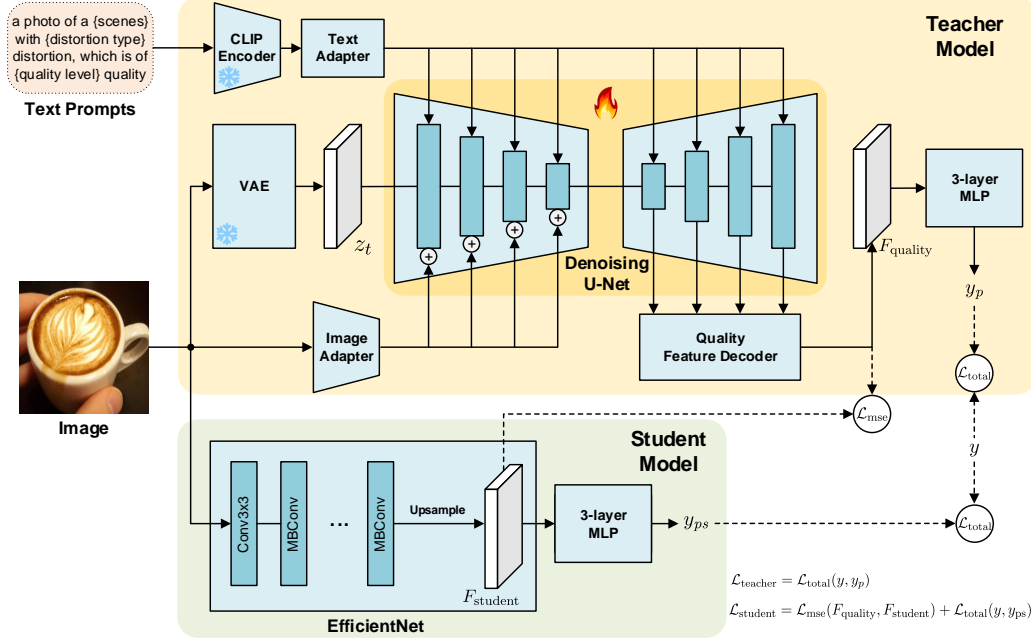


Figure 1: Framework of DP-IQA and its knowledge distillation. DP-IQA is the teacher model, which assesses image quality based on the features extracted from the pre-trained denoising U-Net at a single timestep. Then, we distill the knowledge from DP-IQA into a student model with EfficientNet as the backbone to reduce the parameter. The loss functions are detailed in equation (11) and (12).

distortion and open-world complex authentic distortion and get rid of the reliance on the **patch assemble architecture**. In detail, the framework of our proposed DP-IQA is illustrated in Figure 1. Initially, the input image is encoded with a pre-trained VAE, then fed into the denoising U-Net of the pre-trained stable diffusion [41]. Concurrently, a CLIP encoder [39] converts text describing the image quality into conditional embeddings for the denoising U-Net. The input text is templated and consistent across all images. Meanwhile, text and image adapters are adopted to mitigate the domain gap for downstream tasks and correct the information loss caused by the VAE bottleneck. Subsequently, we extract feature maps from each stage of the U-Net’s upsampling process, which are then fused and decoded by a well-designed Quality Feature Decoder (QFD). Finally, a Multi-Layer Perceptron (MLP) is employed to regress the image quality scores. Figure 2 provides details on the adapters and QFD. Following this, we distill the knowledge in the trained DP-IQA into an EfficientNet-based [50] student model, which is initialized with the official pre-trained weights, and its output structure is modified to align with the teacher model. The distillation process leverages two sources of supervision: (1) the output feature map from the QFD, and (2) the GT image quality scores.

3.3 Diffusion prior-based IQA (DP-IQA)

Extracting diffusion priors. A pre-trained diffusion model contains sufficient information to sample from the data distribution, including its low-level features and structures, as the model can be viewed as the learned gradient of data density [63]. With limited natural language supervision during pre-training, the text-to-image (T2I) model also incorporates significant high-level knowledge. We utilize the pre-trained T2I model stable diffusion [41] as our backbone. In the diffusion process, as the timestep decreases, noise is progressively reduced, demanding the model to recover fine details and complex structures. Hence, the diffusion priors slightly vary with different timesteps. However, using priors across all timesteps results in excessive redundancy, so we select a single timestep t . For an input image $x \in \mathbb{R}^{H \times W \times 3}$, it is encoded into latent representation z_t by a pre-trained VAE. Then, from $\epsilon_\theta(z_t, t)$, we obtain the feature maps f_{up}^i at each upsampling stage, where $i = 1, 2, 3, 4$. The resulting set of feature maps $F_{up}^t = \{f_{up}^{t,1}, f_{up}^{t,2}, f_{up}^{t,3}, f_{up}^{t,4}\}$ is the prior features at timestep t .

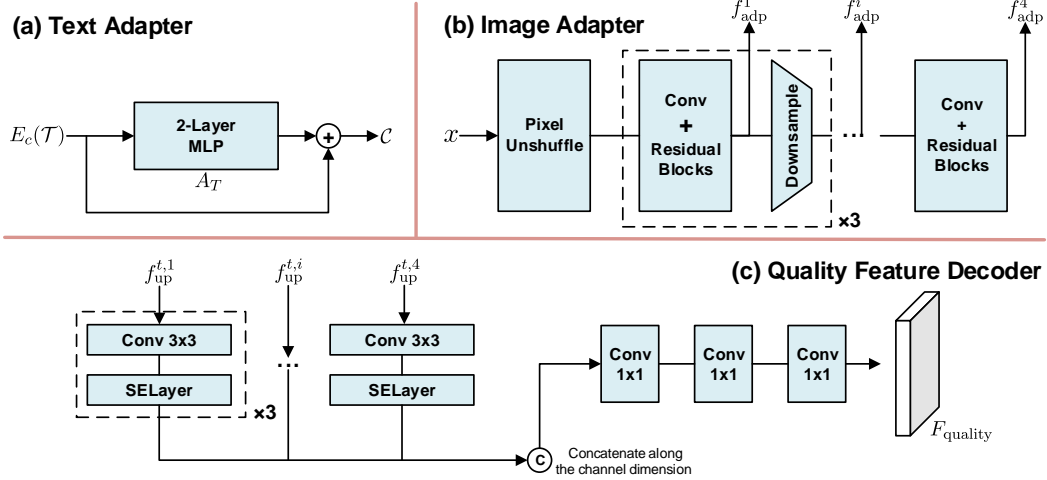


Figure 2: Details of (a) text adapter, (b) image adapter [35] and (c) quality feature decoder in DP-IQA.

Text prompt. In a T2I diffusion model, text is converted into conditional embeddings by a text encoder to guide the denoising process. Stable diffusion uses a CLIP encoder [39] for embedding text. An appropriate text prompt is crucial for the denoiser to focus on the target features. Inspired by [61], we use a general text template to describe the image’s content and quality as the text conditional input. The template is “a photo of a {scenes} with {distortion type} distortion, which is of {quality level} quality.” {Scenes} includes typical image subjects, {distortion type} covers common distortions, and {quality level} provides a general quality description, like “bad” or “good”. Both scenes and distortion types also offer general descriptions. For example, “a photo of an animal with blur distortion, which is of good quality.” Considering that text descriptions cannot cover all possibilities, we suggest including “other” for both scenes and distortion types. Assuming there are l_s scenes, l_d distortion types, and l_q quality levels, there are a total of $k = l_s \cdot l_d \cdot l_q$ combinations. We define \mathcal{T} as the set of all text description combinations.

Text adapter. Due to the domain gap is observed when transferring the text encoder to downstream tasks, a text adapter is commonly used to address this issue [11, 63, 64]. Define the output dimension of the CLIP encoder E_C as d , we can get the original text conditional embedding $E_C(\mathcal{T}) \in \mathbb{R}^{k \times d}$, which is obtained by concatenating the pooled outputs of E_C for all k sentences in \mathcal{T} , and we provide more details about the pooling process in Appendix A. The text adapter consists of a two-layer MLP A_T , and takes $E_C(\mathcal{T})$ as input. The output of A_T is then added to $E_C(\mathcal{T})$ to obtain the adjusted text conditional embedding $\mathcal{C} \in \mathbb{R}^{k \times d}$. This process is:

$$\mathcal{C} = E_C(\mathcal{T}) + A_T(E_C(\mathcal{T})). \quad (5)$$

Image adapter. Since the VAE has not been specifically trained on distorted images, it may inadequately encode distorted content, risking the loss of distortion information when encoding images into latent space. Retraining a VAE on distorted images is overly expensive, so we use an image adapter A_I to extract additional features from the image x . It feeds into the denoising U-Net’s downsampling process, which initially used to control low-level details in T2I generation [35]. We believe it has the potential to supplement low-level distortion information. The image adapter comprises pixel unshuffle, four feature extraction blocks, and three downsampling blocks. Pixel unshuffle downsamples the input to fit the latent space size. Each extraction block has one convolution layer and two residual blocks, while downsampling blocks adjust feature resolution to align with the denoising U-Net’s downsampling feature maps. Define the feature map at each downsampling stage of the denoising U-Net as f_{down}^i , where $i = 1, 2, 3, 4$. The set of downsampling feature maps at timestep t is $F_{\text{down}}^t = \{f_{\text{down}}^{t,1}, f_{\text{down}}^{t,2}, f_{\text{down}}^{t,3}, f_{\text{down}}^{t,4}\}$. Define the output of the image adapter as $A_I(x) = F_{\text{adp}}^i = \{f_{\text{adp}}^1, f_{\text{adp}}^2, f_{\text{adp}}^3, f_{\text{adp}}^4\}$, which is independent of the timestep t , and the size of f_{adp}^i is consistent with $f_{\text{down}}^{t,i}$. The process of feature supplementation by the image adapter is:

$$F_{\text{down}}^{t,i} = F_{\text{down}}^{t,i} + F_{\text{adp}}^i, \quad i = 1, 2, 3, 4. \quad (6)$$

Quality feature decoder (QFD). We design a CNN-based QFD D to decode the feature maps from the upsampling stages, and then regress the output of the decoder through an MLP to obtain the image quality score. The QFD first accepts all four feature maps $f_{\text{up}}^{t,1}, f_{\text{up}}^{t,2}, f_{\text{up}}^{t,3}, f_{\text{up}}^{t,4}$ in F_{up}^t as input, and upsamples all feature maps to a size of 64×64 . Next, a convolution layer and a squeeze-and-excite layer (SELayer) are used to unify the channel number to 512 for each feature map, and the four feature maps are concatenated into a single feature map with 2048 channels. This concatenated feature map is then processed through four convolution layers to gradually reduce the number of channels to 512, 128, 32, and 8. The QFD finally outputs an image quality feature map of size $64 \times 64 \times 8$ as $F_{\text{quality}} = D(F_{\text{up}}^t)$. The F_{quality} is flattened into a one-dimensional vector and passed through a regression network R , which consists of a three-layer MLP, to perform score regression and obtain the predicted value y_p . The process is as follows:

$$F_{\text{quality}} = D(F_{\text{up}}^t) = D(f_{\text{up}}^{t,1}, f_{\text{up}}^{t,2}, f_{\text{up}}^{t,3}, f_{\text{up}}^{t,4}), \quad (7)$$

$$y_p = R(\text{Flatten}(F_{\text{quality}})). \quad (8)$$

Model optimization. Our model is trained in an end-to-end manner. The loss function consists of Mean Squared Error (MSE) loss \mathcal{L}_{mse} and Margin loss $\mathcal{L}_{\text{margin}}$, which are commonly used for learning image quality score regression and ranking (i.e., distinguishing the quality relationship within a batch) in IQA. Assuming the batch size is n , the GT image quality score is y , the predicted value is y_p , and the standard deviation of y is σ_y , the loss functions are as follows:

$$\mathcal{L}_{\text{mse}}(y, y_p) = \frac{1}{n} \|y - y_p\|_2^2, \quad (9)$$

$$\mathcal{L}_{\text{margin}}(y, y_p) = \frac{2}{n(n-1)} \sum_{i < j} \max(0, -\text{sign}(y_i - y_j) \cdot (y_{p_i} - y_{p_j}) + \text{margin}), \quad (10)$$

where $\text{margin} = \lambda \sigma_y$, $\lambda \in [0, 1]$. Therefore, the overall loss function $\mathcal{L}_{\text{total}}$ can be defined as:

$$\mathcal{L}_{\text{total}}(y, y_p) = \mathcal{L}_{\text{mse}}(y, y_p) + \mathcal{L}_{\text{margin}}(y, y_p). \quad (11)$$

In the following text, this model will be referred to as the ‘‘teacher model’’, and its loss function can also be written as $\mathcal{L}_{\text{teacher}}(y, y_p) = \mathcal{L}_{\text{total}}(y, y_p)$.

3.4 Knowledge distillation

Student model. Due to the diffusion model’s numerous parameters, its computational cost is high, hindering its wide deployment in real-world scenarios. Assuming that not all diffusion priors are crucial for IQA, we aim to distill the DP-IQA’s knowledge into a smaller pre-trained vision model. Here, the DP-IQA serves as the teacher model, while the EfficientNet acts as the student. The student model is initialized with official pre-trained weights and its output structure is adjusted to align with the teacher’s. EfficientNet is primarily built with mobile inverted bottleneck convolution (MBConv) [50] and pre-trained for classification, thus it includes high-level priors. The distillation aims to supplement the low-level information it lacks and further enrich its high-level information.

Model optimization. The student model takes the image as input and uses the output feature map F_{quality} from the QFD as supervision to distill the image quality knowledge learned by the teacher model. Additionally, the student model is supervised by the GT image quality score y . Assuming the last feature map before the output layer of the student model is F_{student} , the predicted value of student model is y_{ps} , the loss function $\mathcal{L}_{\text{student}}$ for the student model can be defined as:

$$\mathcal{L}_{\text{student}}(F_{\text{quality}}, F_{\text{student}}, y, y_{\text{ps}}) = \mathcal{L}_{\text{mse}}(F_{\text{quality}}, F_{\text{student}}) + \mathcal{L}_{\text{total}}(y, y_{\text{ps}}) \quad (12)$$

4 Experiment

4.1 Datasets and evaluation metrics

Datasets. IQA datasets primarily consist of distorted images paired with quality scores. We assess our proposed method using four in-the-wild IQA datasets: CLIVE [14], KonIQ [20], LIVEFB [57], and SPAQ [8], which encompass a wide range of authentically distorted images. We also conduct experiments on four synthetically distorted datasets: LIVE [47], CSIQ [26], TID2013 [37], and

Table 1: Comparison of our proposed DP-IQA with SOTA BIQA algorithms on authentically and synthetically distorted datasets. Bold entries and underlined entries are the best performers and second-best performers, respectively.

| Distortion | Authentic (in-the-wild images) | | | | | | | | Synthetic | | | | | | | |
|---------------|--------------------------------|--------------|--------------|--------------|--------------|--------------|--------------|--------------|--------------|--------------|--------------|--------------|--------------|--------------|--------------|--------------|
| Dataset | CLIVE | | KonIQ | | LIVEFB | | SPAQ | | LIVE | | CSIQ | | TID2013 | | KADID | |
| Metrics | PLCC | SRCC | PLCC | SRCC | PLCC | SRCC | PLCC | SRCC | PLCC | SRCC | PLCC | SRCC | PLCC | SRCC | PLCC | SRCC |
| DIIVINE [43] | 0.591 | 0.588 | 0.558 | 0.546 | 0.187 | 0.092 | 0.660 | 0.599 | 0.908 | 0.892 | 0.776 | 0.804 | 0.567 | 0.643 | 0.435 | 0.413 |
| BRISQUE [32] | 0.629 | 0.629 | 0.685 | 0.681 | 0.341 | 0.303 | 0.817 | 0.809 | 0.944 | 0.929 | 0.748 | 0.812 | 0.571 | 0.626 | 0.567 | 0.528 |
| ILNIQE [59] | 0.508 | 0.508 | 0.537 | 0.523 | 0.332 | 0.294 | 0.712 | 0.713 | 0.906 | 0.902 | 0.865 | 0.822 | 0.648 | 0.521 | 0.558 | 0.534 |
| BIECON [24] | 0.613 | 0.613 | 0.654 | 0.651 | 0.428 | 0.407 | - | - | 0.961 | 0.958 | 0.823 | 0.815 | 0.762 | 0.717 | 0.648 | 0.623 |
| MEON [30] | 0.710 | 0.697 | 0.628 | 0.611 | 0.394 | 0.365 | - | - | 0.955 | 0.951 | 0.864 | 0.852 | 0.824 | 0.808 | 0.691 | 0.604 |
| WaDIQA-M [4] | 0.671 | 0.682 | 0.807 | 0.804 | 0.467 | 0.455 | - | - | 0.955 | 0.960 | 0.844 | 0.852 | 0.855 | 0.835 | 0.752 | 0.739 |
| DBCNN [60] | 0.869 | 0.851 | 0.884 | 0.875 | 0.551 | 0.545 | 0.915 | 0.911 | 0.971 | 0.968 | 0.959 | 0.946 | 0.865 | 0.816 | 0.856 | 0.851 |
| TIQA [58] | 0.861 | 0.845 | 0.903 | 0.892 | 0.581 | 0.541 | - | - | 0.965 | 0.949 | 0.838 | 0.825 | 0.858 | 0.846 | 0.855 | 0.850 |
| MetalQA [65] | 0.802 | 0.835 | 0.856 | 0.887 | 0.507 | 0.540 | - | - | 0.959 | 0.960 | 0.908 | 0.899 | 0.868 | 0.856 | 0.775 | 0.762 |
| P2P-BM [57] | 0.842 | 0.844 | 0.885 | 0.872 | 0.598 | 0.526 | - | - | 0.958 | 0.959 | 0.902 | 0.899 | 0.856 | 0.862 | 0.849 | 0.840 |
| HyperIQA [49] | 0.882 | 0.859 | 0.917 | 0.906 | 0.602 | 0.544 | 0.915 | 0.911 | 0.966 | 0.962 | 0.942 | 0.923 | 0.858 | 0.840 | 0.845 | 0.852 |
| MUSIQ [23] | 0.746 | 0.702 | 0.928 | 0.916 | 0.661 | 0.566 | 0.921 | 0.918 | 0.911 | 0.940 | 0.893 | 0.871 | 0.815 | 0.773 | 0.872 | 0.875 |
| TReS [16] | 0.877 | 0.846 | 0.928 | 0.915 | 0.625 | 0.554 | - | - | 0.968 | 0.969 | 0.942 | 0.922 | 0.883 | 0.863 | 0.858 | 0.859 |
| DEIQT [38] | 0.886 | 0.861 | 0.934 | 0.921 | 0.645 | 0.557 | 0.921 | 0.914 | 0.957 | 0.953 | 0.951 | 0.934 | 0.853 | 0.823 | 0.878 | 0.880 |
| RelQA [45] | 0.854 | 0.840 | 0.923 | 0.914 | - | - | 0.925 | 0.918 | 0.972 | 0.971 | 0.964 | 0.947 | 0.880 | 0.844 | 0.892 | 0.885 |
| Ours(student) | 0.902 | 0.875 | 0.933 | 0.920 | 0.666 | 0.566 | 0.923 | 0.920 | 0.951 | 0.945 | 0.928 | 0.915 | 0.892 | 0.867 | 0.907 | 0.911 |
| Ours(teacher) | 0.907 | 0.879 | 0.951 | 0.942 | 0.664 | 0.551 | 0.926 | 0.923 | 0.941 | 0.939 | 0.915 | 0.902 | 0.895 | 0.881 | 0.888 | 0.888 |

Table 2: Comparison of SRCC on cross datasets. Bold entries and underlined entries are the best performers and second-best performers, respectively.

| Training on | LIVEFB | | CLIVE | KonIQ |
|---------------|--------------|--------------|--------------|--------------|
| Testing on | KonIQ | CLIVE | KonIQ | CLIVE |
| DBCNN | 0.716 | 0.724 | 0.754 | 0.755 |
| P2P-BM | 0.755 | 0.738 | 0.740 | 0.770 |
| HyperIQA | 0.758 | 0.735 | 0.772 | 0.785 |
| TReS | 0.713 | 0.740 | 0.733 | 0.786 |
| Ours(student) | 0.767 | 0.758 | 0.781 | 0.830 |
| Ours(teacher) | 0.767 | 0.770 | 0.738 | 0.833 |

KADID [28], to explore the potential applicability of our method to synthetic distortions, although this is not our primary focus. Synthetic images are derived from a limited number of reference photos, restricting content diversity. For instance, the largest synthetic dataset, KADID-10k, is based on only 81 reference images and a limited combination of applied distortions, which do not reflect the authentic distortions commonly seen in publicly available images, such as focus errors or motion blur due to object movement [20]. Consequently, our study primarily emphasizes authentic distortions. Further details about the datasets we used are presented in Appendix B.

Evaluation metrics. Consistent with other works, we use Pearson’s linear correlation coefficient (PLCC) and Spearman’s rank-order correlation coefficient (SRCC) as performance evaluation metrics. Their values range from 0 to 1, and a higher value indicates better performance.

4.2 Implementation

We implement our model using PyTorch and conduct training and testing on an A100 GPU. The version of stable diffusion is v1.5, while EfficientNet-B7 served as the backbone for the student model. We use Adam as the optimizer. The teacher model DP-IQA (1.19B parameters) is trained with a batch size of at least 12, an initial learning rate of 10^{-5} , for up to 15 epochs, while the student model (81.01M parameters) with 24, 10^{-4} and 30, respectively. Learning rate decay differ slightly across datasets, as detailed in Appendix C. We also provide more detailed settings in Appendix D.

For data preprocessing, we simply resize in-the-wild images to 512×512 pixels. However, synthetic datasets still require splitting images into two patches; images are resized to 1024×768 and then divided into two 512×512 patches. This is because synthetic datasets have very low diversity, leading to similar content distributions and causing large models to overfit easily. We randomly split datasets

Table 3: Ablation analysis of text prompt (TP), text adapter(TA) and image adapter(IA) in teacher model. Bold entries are the best performers.

| Dataset | Full | | w/o TP | | w/o TA | | w/o IA | |
|---------|--------------|--------------|--------|-------|--------|-------|--------|-------|
| | PLCC | SRCC | PLCC | SRCC | PLCC | SRCC | PLCC | SRCC |
| CLIVE | 0.907 | 0.879 | 0.904 | 0.896 | 0.867 | 0.871 | 0.901 | 0.875 |
| KonIQ | 0.951 | 0.942 | 0.941 | 0.940 | 0.929 | 0.931 | 0.946 | 0.932 |

Table 4: Ablation analysis of the settings of timestep for teacher model. Bold entries are the best performers.

| Dataset | Timestep | | | | | | | | | | | |
|---------|--------------|--------------|--------------|-------|--------------|-------|-------|-------|--------------|-------|-------|-------|
| | 1 | | 3 | | 5 | | 10 | | 20 | | 50 | |
| | PLCC | SRCC | PLCC | SRCC | PLCC | SRCC | PLCC | SRCC | PLCC | SRCC | PLCC | SRCC |
| CLIVE | 0.907 | 0.879 | 0.907 | 0.865 | 0.907 | 0.859 | 0.906 | 0.865 | 0.907 | 0.865 | 0.903 | 0.873 |
| KonIQ | 0.951 | 0.942 | 0.948 | 0.940 | 0.947 | 0.939 | 0.945 | 0.936 | 0.946 | 0.936 | 0.942 | 0.931 |

Table 5: Ablation analysis of distillation, where stud. means student model. Bold entries are the best performers, and “stud.” is the abbreviation for student model.

| Dataset | Distilled stud. | | w/o distillation | |
|---------|-----------------|--------------|------------------|-------|
| | PLCC | SRCC | PLCC | SRCC |
| CLIVE | 0.902 | 0.875 | 0.717 | 0.715 |
| KonIQ | 0.933 | 0.920 | 0.881 | 0.841 |

into training and testing sets in 8:2. For in-the-wild datasets, we split across all images, while synthetic datasets are split based on reference images. We repeated the splitting process five times for all datasets and reported the median results. We show standard deviation of the results in Appendix E.

4.3 Comparison against other methods

Overall comparison. We compare our method with 15 SOTA baselines. Table 1 shows the overall performance comparison in terms of PLCC and SRCC across 8 standard IQA datasets. The data of ReIQA [45] is sourced from its original paper, DEIQT [38] is based on our reproduction, and other data are from [16] and [38]. The experimental results indicate that our method achieved the best performance on all the in-the-wild image datasets we used. Moreover, for synthetic distortion, it also performed best on larger datasets such as TID2013 and KADID. The results demonstrate that our method excels in assessing the quality of authentically distorted images from in-the-wild datasets and shows considerable potential for quality evaluation of synthetically distorted images, although it demands datasets of larger scale and better diversity.

Generalization. In Table 2, to test the model’s generalization capability for authentic distortion, we conduct cross-dataset zero-shot performance evaluations on three in-the-wild datasets. Following other works, we use SRCC as the evaluation metric. Since different synthetically distorted datasets have significant differences in scoring systems and types of distortion, and are irrelevant to our design objectives, they are not considered. In this experiment, only the training sets of the respective datasets are used for training, while testing is conducted on the complete datasets. We compare our method with other SOTA baselines that have reported model generalization capability, and the experimental results show that our method currently has the best generalization capability.

4.4 Ablation

Due to the high cost of conducting experiments on SPAQ and LIVEFB, ablation experiments are primarily conducted on CLIVE and KonIQ. Our ablation experiments include the main components affecting model performance in the teacher model, such as text prompt, text adapter, image adapter, and the settings of timestep, as well as the knowledge distillation process.



Figure 3: Examples of DP-IQA and its student model applied to in-the-wild images from KonIQ dataset. Colored fonts represent the deviation between predicted values and ground truth (GT) scores, with red indicating good predictions and blue indicating results with larger errors.

Text prompt and adapters. As shown in Table 3, we explore the impact of text prompt on model performance. Additionally, we also conduct ablation studies on the text adapter and image adapter. When there is no text prompt (w/o TP), the text adapter was not activated by default. The results indicate that the text adapter, image adapter, and text prompt play positive roles in overall performance.

Timesteps. As shown in Table 4, we observe the impact of different timestep settings on model performance. The results show that using smaller timesteps is generally more advantageous.

Distillation. As shown in Table 5, we conduct ablation analysis on the distillation process. Experimental results indicate that distillation effectively enhances the performance of the student model. This also demonstrates that the outstanding performance of the student model does not solely rely on its own model architecture design and pre-trained weights.

4.5 Discussion of limitation

Figure 4 presents examples of our DP-IQA and its student model applied to in-the-wild images, including both accurate predictions and results with larger errors. The scores are normalized to a range of 0 to 1, where higher scores indicate better quality. DP-IQA and its student model generally performs well across various subjects and quality levels. However, for images with hard-to-distinguish scenes or objects, its predictions may deviate. This might be due to insufficient training data. Additionally, the predictions of student model occasionally deviates significantly from its teachers'. Nevertheless, due to the limited samples of this situation, it is difficult to observe a pattern.

5 Conclusion

In this paper, we propose a novel BIQA method based on diffusion model priors for in-the-wild images, named DP-IQA. DP-IQA addresses the non-uniform distribution of distortions in in-the-wild images by leveraging the excellent global modeling capabilities of diffusion model for image-level modeling, rather than performing patch splitting on in-the-wild images. Additionally, the introduction of large-scale pre-trained stable diffusion priors compensates for the neglect of low-level priors seen in previous methods using pre-trained classification networks. To alleviate the computational burden of diffusion models in practical applications, we also distill the knowledge from DP-IQA into a smaller EfficientNet-based student model. Experimental results show that DP-IQA achieves SOTA results on various in-the-wild datasets and demonstrates the best generalization capabilities.

References

- [1] Dmitry Baranchuk, Ivan Rubachev, Andrey Voynov, Valentin Khrukov, and Artem Babenko. Label-efficient semantic segmentation with diffusion models. *arXiv preprint arXiv:2112.03126*, 2021.
- [2] Simone Bianco, Luigi Celona, Paolo Napoletano, and Raimondo Schettini. On the use of deep learning for blind image quality assessment. *Signal, Image and Video Processing*, 12:355–362, 2018.
- [3] Sebastian Bosse, Dominique Maniry, Klaus-Robert Müller, Thomas Wiegand, and Wojciech Samek. Deep neural networks for no-reference and full-reference image quality assessment. *IEEE Transactions on image processing*, 27(1):206–219, 2017.
- [4] Sebastian Bosse, Dominique Maniry, Klaus-Robert Müller, Thomas Wiegand, and Wojciech Samek. Deep neural networks for no-reference and full-reference image quality assessment. *IEEE Transactions on image processing*, 27(1):206–219, 2017.
- [5] Tai-Yin Chiu, Yinan Zhao, and Danna Gurari. Assessing image quality issues for real-world problems. In *proceedings of the IEEE/CVF conference on computer vision and pattern recognition*, pages 3646–3656, 2020.
- [6] Jia Deng, Wei Dong, Richard Socher, Li-Jia Li, Kai Li, and Li Fei-Fei. Imagenet: A large-scale hierarchical image database. In *2009 IEEE conference on computer vision and pattern recognition*, pages 248–255. Ieee, 2009.
- [7] Alexey Dosovitskiy, Lucas Beyer, Alexander Kolesnikov, Dirk Weissenborn, Xiaohua Zhai, Thomas Unterthiner, Mostafa Dehghani, Matthias Minderer, Georg Heigold, Sylvain Gelly, et al. An image is worth 16x16 words: Transformers for image recognition at scale. *arXiv preprint arXiv:2010.11929*, 2020.
- [8] Yuming Fang, Hanwei Zhu, Yan Zeng, Kede Ma, and Zhou Wang. Perceptual quality assessment of smartphone photography. In *Proceedings of the IEEE/CVF conference on computer vision and pattern recognition*, pages 3677–3686, 2020.
- [9] Ben Fei, Zhaoyang Lyu, Liang Pan, Junzhe Zhang, Weidong Yang, Tianyue Luo, Bo Zhang, and Bo Dai. Generative diffusion prior for unified image restoration and enhancement. In *Proceedings of the IEEE/CVF Conference on Computer Vision and Pattern Recognition*, pages 9935–9946, 2023.
- [10] Fei Gao, Jun Yu, Suguo Zhu, Qingming Huang, and Qi Tian. Blind image quality prediction by exploiting multi-level deep representations. *Pattern Recognition*, 81:432–442, 2018.
- [11] Peng Gao, Shijie Geng, Renrui Zhang, Teli Ma, Rongyao Fang, Yongfeng Zhang, Hongsheng Li, and Yu Qiao. Clip-adapter: Better vision-language models with feature adapters. *International Journal of Computer Vision*, 132(2):581–595, 2024.
- [12] Xinbo Gao, Fei Gao, Dacheng Tao, and Xuelong Li. Universal blind image quality assessment metrics via natural scene statistics and multiple kernel learning. *IEEE Transactions on neural networks and learning systems*, 24(12), 2013.
- [13] Deepti Ghadiyaram and Alan C Bovik. Blind image quality assessment on real distorted images using deep belief nets. In *2014 IEEE global conference on signal and information processing (GlobalSIP)*, pages 946–950. IEEE, 2014.
- [14] Deepti Ghadiyaram and Alan C Bovik. Massive online crowdsourced study of subjective and objective picture quality. *IEEE Transactions on Image Processing*, 25(1):372–387, 2015.
- [15] Deepti Ghadiyaram and Alan C Bovik. Perceptual quality prediction on authentically distorted images using a bag of features approach. *Journal of vision*, 17(1):32–32, 2017.
- [16] S Alireza Golestaneh, Saba Dadsetan, and Kris M Kitani. No-reference image quality assessment via transformers, relative ranking, and self-consistency. In *Proceedings of the IEEE/CVF winter conference on applications of computer vision*, pages 1220–1230, 2022.

- [17] Lanqing Guo, Chong Wang, Wenhan Yang, Siyu Huang, Yufei Wang, Hanspeter Pfister, and Bihan Wen. Shadowdiffusion: When degradation prior meets diffusion model for shadow removal. In *Proceedings of the IEEE/CVF Conference on Computer Vision and Pattern Recognition*, pages 14049–14058, 2023.
- [18] Kaiming He, Xiangyu Zhang, Shaoqing Ren, and Jian Sun. Deep residual learning for image recognition. In *Proceedings of the IEEE conference on computer vision and pattern recognition*, pages 770–778, 2016.
- [19] Jonathan Ho, Ajay Jain, and Pieter Abbeel. Denoising diffusion probabilistic models. *Advances in neural information processing systems*, 33:6840–6851, 2020.
- [20] Vlad Hosu, Hanhe Lin, Tamas Sziranyi, and Dietmar Saupe. Koniq-10k: An ecologically valid database for deep learning of blind image quality assessment. *IEEE Transactions on Image Processing*, 29:4041–4056, 2020.
- [21] Le Kang, Peng Ye, Yi Li, and David Doermann. Convolutional neural networks for no-reference image quality assessment. In *Proceedings of the IEEE conference on computer vision and pattern recognition*, pages 1733–1740, 2014.
- [22] Bingxin Ke, Anton Obukhov, Shengyu Huang, Nando Metzger, Rodrigo Caye Daudt, and Konrad Schindler. Repurposing diffusion-based image generators for monocular depth estimation. *arXiv preprint arXiv:2312.02145*, 2023.
- [23] Junjie Ke, Qifei Wang, Yilin Wang, Peyman Milanfar, and Feng Yang. Musiq: Multi-scale image quality transformer. In *Proceedings of the IEEE/CVF international conference on computer vision*, pages 5148–5157, 2021.
- [24] Jongyoo Kim and Sanghoon Lee. Fully deep blind image quality predictor. *IEEE Journal of selected topics in signal processing*, 11(1):206–220, 2016.
- [25] Jongyoo Kim, Hui Zeng, Deepti Ghadiyaram, Sanghoon Lee, Lei Zhang, and Alan C Bovik. Deep convolutional neural models for picture-quality prediction: Challenges and solutions to data-driven image quality assessment. *IEEE Signal processing magazine*, 34(6):130–141, 2017.
- [26] Eric C Larson and Damon M Chandler. Most apparent distortion: full-reference image quality assessment and the role of strategy. *Journal of electronic imaging*, 19(1):011006–011006, 2010.
- [27] Alexander C Li, Mihir Prabhudesai, Shivam Duggal, Ellis Brown, and Deepak Pathak. Your diffusion model is secretly a zero-shot classifier. In *Proceedings of the IEEE/CVF International Conference on Computer Vision*, pages 2206–2217, 2023.
- [28] Hanhe Lin, Vlad Hosu, and Dietmar Saupe. Kadid-10k: A large-scale artificially distorted iqa database. In *2019 Eleventh International Conference on Quality of Multimedia Experience (QoMEX)*, pages 1–3. IEEE, 2019.
- [29] Kwan-Yee Lin and Guanxiang Wang. Hallucinated-iqa: No-reference image quality assessment via adversarial learning. In *Proceedings of the IEEE conference on computer vision and pattern recognition*, pages 732–741, 2018.
- [30] Kede Ma, Wentao Liu, Kai Zhang, Zhengfang Duanmu, Zhou Wang, and Wangmeng Zuo. End-to-end blind image quality assessment using deep neural networks. *IEEE Transactions on Image Processing*, 27(3):1202–1213, 2017.
- [31] Pavan C Madhusudana, Neil Birkbeck, Yilin Wang, Balu Adsumilli, and Alan C Bovik. Image quality assessment using contrastive learning. *IEEE Transactions on Image Processing*, 31: 4149–4161, 2022.
- [32] Anish Mittal, Anush Krishna Moorthy, and Alan Conrad Bovik. No-reference image quality assessment in the spatial domain. *IEEE Transactions on image processing*, 21(12):4695–4708, 2012.
- [33] Anush Krishna Moorthy and Alan Conrad Bovik. A two-step framework for constructing blind image quality indices. *IEEE Signal processing letters*, 17(5):513–516, 2010.

- [34] Anush Krishna Moorthy and Alan Conrad Bovik. Blind image quality assessment: From natural scene statistics to perceptual quality. *IEEE transactions on Image Processing*, 20(12): 3350–3364, 2011.
- [35] Chong Mou, Xintao Wang, Liangbin Xie, Yanze Wu, Jian Zhang, Zhongang Qi, and Ying Shan. T2i-adapter: Learning adapters to dig out more controllable ability for text-to-image diffusion models. In *Proceedings of the AAAI Conference on Artificial Intelligence*, pages 4296–4304, 2024.
- [36] Da Pan, Ping Shi, Ming Hou, Zefeng Ying, Sizhe Fu, and Yuan Zhang. Blind predicting similar quality map for image quality assessment. In *Proceedings of the IEEE conference on computer vision and pattern recognition*, pages 6373–6382, 2018.
- [37] Nikolay Ponomarenko, Lina Jin, Oleg Ieremeiev, Vladimir Lukin, Karen Egiazarian, Jaakko Astola, Benoit Vozel, Kacem Chehdi, Marco Carli, Federica Battisti, et al. Image database tid2013: Peculiarities, results and perspectives. *Signal processing: Image communication*, 30: 57–77, 2015.
- [38] Guanyi Qin, Runze Hu, Yutao Liu, Xiawu Zheng, Haotian Liu, Xiu Li, and Yan Zhang. Data-efficient image quality assessment with attention-panel decoder. In *Proceedings of the AAAI Conference on Artificial Intelligence*, pages 2091–2100, 2023.
- [39] Alec Radford, Jong Wook Kim, Chris Hallacy, Aditya Ramesh, Gabriel Goh, Sandhini Agarwal, Girish Sastry, Amanda Askell, Pamela Mishkin, Jack Clark, et al. Learning transferable visual models from natural language supervision. In *International conference on machine learning*, pages 8748–8763. PMLR, 2021.
- [40] Hongyu Ren, Diqi Chen, and Yizhou Wang. Ran4iqa: Restorative adversarial nets for no-reference image quality assessment. In *Proceedings of the AAAI conference on artificial intelligence*, 2018.
- [41] Robin Rombach, Andreas Blattmann, Dominik Lorenz, Patrick Esser, and Björn Ommer. High-resolution image synthesis with latent diffusion models. In *Proceedings of the IEEE/CVF conference on computer vision and pattern recognition*, pages 10684–10695, 2022.
- [42] Michele A Saad, Alan C Bovik, and Christophe Charrier. A dct statistics-based blind image quality index. *IEEE Signal Processing Letters*, 17(6):583–586, 2010.
- [43] Michele A Saad, Alan C Bovik, and Christophe Charrier. Blind image quality assessment: A natural scene statistics approach in the dct domain. *IEEE transactions on Image Processing*, 21(8):3339–3352, 2012.
- [44] Andleeb Sadiq, Imran Fareed Nizami, Syed Muhammad Anwar, and Muhammad Majid. Blind image quality assessment using natural scene statistics of stationary wavelet transform. *Optik*, 205:164189, 2020.
- [45] Avinab Saha, Sandeep Mishra, and Alan C Bovik. Re-iqa: Unsupervised learning for image quality assessment in the wild. In *Proceedings of the IEEE/CVF Conference on Computer Vision and Pattern Recognition*, pages 5846–5855, 2023.
- [46] Christoph Schuhmann, Romain Beaumont, Richard Vencu, Cade Gordon, Ross Wightman, Mehdi Cherti, Theo Coombes, Aarush Katta, Clayton Mullis, Mitchell Wortsman, et al. Laion-5b: An open large-scale dataset for training next generation image-text models. *Advances in Neural Information Processing Systems*, 35:25278–25294, 2022.
- [47] Hamid R Sheikh, Muhammad F Sabir, and Alan C Bovik. A statistical evaluation of recent full reference image quality assessment algorithms. *IEEE Transactions on image processing*, 15(11):3440–3451, 2006.
- [48] Shaolin Su, Qingsen Yan, Yu Zhu, Cheng Zhang, Xin Ge, Jinqiu Sun, and Yanning Zhang. Blindly assess image quality in the wild guided by a self-adaptive hyper network. In *Proceedings of the IEEE/CVF conference on computer vision and pattern recognition*, pages 3667–3676, 2020.

- [49] Shaolin Su, Qingsen Yan, Yu Zhu, Cheng Zhang, Xin Ge, Jinqiu Sun, and Yanning Zhang. Blindly assess image quality in the wild guided by a self-adaptive hyper network. In *Proceedings of the IEEE/CVF conference on computer vision and pattern recognition*, pages 3667–3676, 2020.
- [50] Mingxing Tan and Quoc Le. Efficientnet: Rethinking model scaling for convolutional neural networks. In *International conference on machine learning*, pages 6105–6114. PMLR, 2019.
- [51] Huixuan Tang, Neel Joshi, and Ashish Kapoor. Blind image quality assessment using semi-supervised rectifier networks. In *proceedings of the IEEE conference on computer vision and pattern recognition*, pages 2877–2884, 2014.
- [52] Junjiao Tian, Lavisha Aggarwal, Andrea Colaco, Zsolt Kira, and Mar Gonzalez-Franco. Diffuse, attend, and segment: Unsupervised zero-shot segmentation using stable diffusion. *arXiv preprint arXiv:2308.12469*, 2023.
- [53] Domonkos Varga, Dietmar Saupe, and Tamás Szirányi. Deepnrn: A content preserving deep architecture for blind image quality assessment. In *2018 IEEE International Conference on Multimedia and Expo (ICME)*, pages 1–6. IEEE, 2018.
- [54] Jianyi Wang, Zongsheng Yue, Shangchen Zhou, Kelvin CK Chan, and Chen Change Loy. Exploiting diffusion prior for real-world image super-resolution. *arXiv preprint arXiv:2305.07015*, 2023.
- [55] Jie Xiao, Ruili Feng, Han Zhang, Zhiheng Liu, Zhantao Yang, Yurui Zhu, Xueyang Fu, Kai Zhu, Yu Liu, and Zheng-Jun Zha. Dreamclean: Restoring clean image using deep diffusion prior. In *The Twelfth International Conference on Learning Representations*.
- [56] Wufeng Xue, Xuanqin Mou, Lei Zhang, Alan C Bovik, and Xiangchu Feng. Blind image quality assessment using joint statistics of gradient magnitude and laplacian features. *IEEE Transactions on Image Processing*, 23(11):4850–4862, 2014.
- [57] Zhenqiang Ying, Haoran Niu, Praful Gupta, Dhruv Mahajan, Deepti Ghadiyaram, and Alan Bovik. From patches to pictures (paq-2-piq): Mapping the perceptual space of picture quality. In *Proceedings of the IEEE/CVF conference on computer vision and pattern recognition*, pages 3575–3585, 2020.
- [58] Junyong You and Jari Korhonen. Transformer for image quality assessment. In *2021 IEEE International Conference on Image Processing (ICIP)*, pages 1389–1393. IEEE, 2021.
- [59] Lin Zhang, Lei Zhang, and Alan C Bovik. A feature-enriched completely blind image quality evaluator. *IEEE Transactions on Image Processing*, 24(8):2579–2591, 2015.
- [60] Weixia Zhang, Kede Ma, jia Yan, Dexiang Deng, and Zhou Wang. Blind image quality assessment using a deep bilinear convolutional neural network. *IEEE Transactions on Circuits and Systems for Video Technology*, 30, 2018.
- [61] Weixia Zhang, Guangtao Zhai, Ying Wei, Xiaokang Yang, and Kede Ma. Blind image quality assessment via vision-language correspondence: A multitask learning perspective. In *Proceedings of the IEEE/CVF conference on computer vision and pattern recognition*, pages 14071–14081, 2023.
- [62] Kai Zhao, Kun Yuan, Ming Sun, Mading Li, and Xing Wen. Quality-aware pre-trained models for blind image quality assessment. In *Proceedings of the IEEE/CVF Conference on Computer Vision and Pattern Recognition*, pages 22302–22313, 2023.
- [63] Wenliang Zhao, Yongming Rao, Zuyan Liu, Benlin Liu, Jie Zhou, and Jiwen Lu. Unleashing text-to-image diffusion models for visual perception. In *Proceedings of the IEEE/CVF International Conference on Computer Vision*, pages 5729–5739, 2023.
- [64] Kaiyang Zhou, Jingkang Yang, Chen Change Loy, and Ziwei Liu. Learning to prompt for vision-language models. *International Journal of Computer Vision*, 130(9):2337–2348, 2022.

- [65] Hancheng Zhu, Leida Li, Jinjian Wu, Weisheng Dong, and Guangming Shi. MetaIqa: Deep meta-learning for no-reference image quality assessment. In *Proceedings of the IEEE/CVF conference on computer vision and pattern recognition*, pages 14143–14152, 2020.
- [66] Yunan Zhu, Haichuan Ma, Jialun Peng, Dong Liu, and Zhiwei Xiong. Recycling discriminator: Towards opinion-unaware image quality assessment using wasserstein gan. In *Proceedings of the 29th ACM International Conference on Multimedia*, pages 116–125, 2021.

A Pooled outputs of CLIP encoder

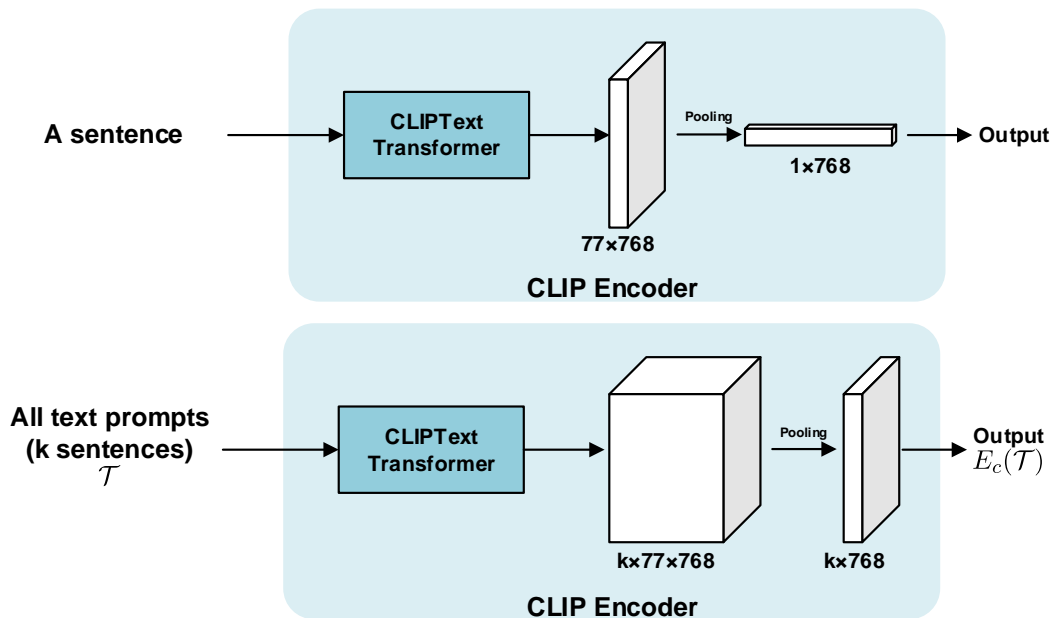


Figure 4: Further explanation of the text embedding process using the CLIP encoder. We demonstrate the pooling process to better understand the changes in data dimensions. For specific variable definitions, please refer to Sec. 3.

B Supplementary information for the IQA datasets

Table 6: Summary of IQA datasets included in our work.

| Dataset | Distortion Type | Number of images | Number of ref. images | Establishment year |
|--------------|-----------------|------------------|-----------------------|--------------------|
| CLIVE [14] | authentic | 1,162 | - | 2016 |
| KonIQ [20] | authentic | 10,073 | - | 2020 |
| SPAQ [8] | authentic | 11,125 | - | 2020 |
| LIVEFB [57] | authentic | 39,810 | - | 2020 |
| LIVE [47] | synthetic | 779 | 29 | 2005 |
| CSIQ [26] | synthetic | 866 | 30 | 2009 |
| TID2013 [37] | synthetic | 3,000 | 25 | 2013 |
| KADID [28] | synthetic | 10,125 | 81 | 2019 |

C Supplementary information on training details

Table 7: Learning rate decay strategies on different datasets, with the data in the table indicating the epochs at which the learning rate is reduced. The scheduler used is MultiStepLR, with a decay factor of 0.2.

| Dataset | CLIVE | KonIQ | LIVEFB | SPAQ | LIVE | CSIQ | TID2013 | KADID |
|---------------|--------|-------|--------|------|--------|--------|---------|-------|
| Teacher model | - | 5 | 2 | - | 2 | 2, 4 | - | 5 |
| Student model | 10, 25 | 5 | 4 | 6 | 10, 25 | 10, 25 | 3, 10 | 5, 10 |

D Supplementary information for experiment implementation

Table 8: Details of the text prompt template we used in the experiment.

| Word types | Details |
|-----------------|---|
| Scenes | animal cityscape, human, indoor, landscape, night, plant, still_life, other |
| Distortion type | jpeg2000 compression, jpeg compression, noise, blur, color, contrast, overexposure, underexposure, spatial, quantization, other |
| Quality level | bad, poor, fair, good, perfect |

Table 9: The values of the numeric variables defined in Sec. 3.

| Variable | Value | Explanation |
|-----------|-------|--|
| H | 512 | Height of the input image |
| W | 512 | Width of the input image |
| l_s | 11 | The number of elements in {scenes} |
| l_d | 9 | The number of elements in {distortion type} |
| l_q | 5 | The number of elements in {quality level} |
| k | 495 | The total number of combinations of text templates |
| d | 768 | Output dimension of the CLIP encoder |
| λ | 0.25 | Coefficient used to control the margin |

E Standard deviation of the experimental results

Table 10: The standard deviation of the results from Table.1.

| Distortion | Authentic (in-the-wild images) | | | | | | | | Synthetic | | | | | | | |
|---------------|--------------------------------|-------|-------|-------|--------|-------|-------|-------|-----------|-------|-------|-------|---------|-------|-------|-------|
| | CLIVE | | KonIQ | | LIVEFB | | SPAQ | | LIVE | | CSIQ | | TID2013 | | KADID | |
| Dataset | PLCC | SRCC | PLCC | SRCC | PLCC | SRCC | PLCC | SRCC | PLCC | SRCC | PLCC | SRCC | PLCC | SRCC | PLCC | SRCC |
| Ours(student) | 0.002 | 0.009 | 0.002 | 0.003 | 0.007 | 0.006 | 0.002 | 0.003 | 0.014 | 0.011 | 0.008 | 0.009 | 0.038 | 0.038 | 0.005 | 0.006 |
| Ours(teacher) | 0.005 | 0.011 | 0.002 | 0.003 | 0.011 | 0.011 | 0.002 | 0.003 | 0.014 | 0.015 | 0.024 | 0.024 | 0.070 | 0.086 | 0.011 | 0.012 |

Table 11: The standard deviation of the results from Table.2.

| Training on | LIVEFB | | CLIVE | KonIQ |
|---------------|--------|-------|-------|-------|
| Testing on | KonIQ | CLIVE | KonIQ | CLIVE |
| Ours(student) | 0.005 | 0.008 | 0.001 | 0.009 |
| Ours(teacher) | 0.002 | 0.012 | 0.020 | 0.011 |

Table 12: The standard deviation of the results from Table.3.

| Dataset | Full | | w/o TP | | w/o TA | | w/o IA | |
|---------|-------|-------|--------|-------|--------|-------|--------|-------|
| | PLCC | SRCC | PLCC | SRCC | PLCC | SRCC | PLCC | SRCC |
| CLIVE | 0.005 | 0.011 | 0.009 | 0.011 | 0.008 | 0.009 | 0.006 | 0.014 |
| KonIQ | 0.002 | 0.003 | 0.004 | 0.002 | 0.002 | 0.006 | 0.003 | 0.001 |

Table 13: The standard deviation of the results from Table.4.

| Dataset | Timestep | | | | | | | | | | | |
|---------|----------|-------|-------|-------|-------|-------|-------|-------|-------|-------|-------|-------|
| | 1 | | 3 | | 5 | | 10 | | 20 | | 50 | |
| | PLCC | SRCC | PLCC | SRCC | PLCC | SRCC | PLCC | SRCC | PLCC | SRCC | PLCC | SRCC |
| CLIVE | 0.005 | 0.011 | 0.007 | 0.009 | 0.008 | 0.008 | 0.007 | 0.009 | 0.010 | 0.015 | 0.016 | 0.017 |
| KonIQ | 0.002 | 0.003 | 0.002 | 0.004 | 0.003 | 0.004 | 0.003 | 0.004 | 0.004 | 0.004 | 0.004 | 0.010 |

Table 14: The standard deviation of the results from Table.5.

| Dataset | Distilled stud. | | w/o distillation | |
|---------|-----------------|-------|------------------|-------|
| | PLCC | SRCC | PLCC | SRCC |
| CLIVE | 0.002 | 0.009 | 0.013 | 0.022 |
| KonIQ | 0.002 | 0.003 | 0.002 | 0.002 |